https://doi.org/10.5194/egusphere-2026-2014
Preprint. Discussion started: 19 May 2026

Development of a high-resolution coupled SHiELD-MOM6-LM4 model – Part 2: Model overview, coupling technique, and evaluation of hydrological extremes during Hurricane Helene

Joseph Mouallem[1], Sergey Malyshev[2], Zhihong Tan[1], Elena Shevliakova[2], Kun Gao[1], Lucas Harris[2], Rusty Benson[2], William Cooke[2], Niki Zadeh[2], and Lauren Chilutti[2]

[1]Program in Atmospheric and Oceanic Sciences, Princeton University, Princeton, NJ, USA
[2]Geophysical Fluid Dynamics Laboratory/NOAA, Princeton, NJ, USA

Correspondence: J. Mouallem (mouallem@princeton.edu)

Abstract. This work describes the implementation strategy and technical challenges involved in integrating the Geophysical Fluid Dynamics Laboratory (GFDL)'s Land Model (LM4) with dynamic subgrid tiling capabilities within the atmospheric model, System for High-resolution modeling for Earth-to-Local Domains (SHiELD), capable of kilometer-scale global simulations. A key challenge addressed in this effort is coupling LM4, which was designed for implicit surface flux coupling, with SHiELD's explicit physics solver. We achieve this through a refactoring of the atmospheric physics suite and code drivers, enabling implicit land-atmosphere coupling of heat and moisture within the well established FMS coupler infrastructure. The resulting flexible architecture supports multiple model configurations from a single executable without recompilation. This extends SHiELD from an uncoupled atmospheric model, in which land processes are treated as a part of the atmospheric physics package, to a fully coupled high resolution atmosphere-ocean-land-ice model. We demonstrate the new system through a high-resolution global simulation of Hurricane Helene's landfall where the land component realistically captures the rapid soil saturation, localized runoff generation and multi-day river flooding concentration in Western North Carolina. These results validate the technical coupling strategy, unlock new forecast capabilities, and highlight the importance of interactive land-atmosphere coupling for simulating extreme weather and hydrological events.

1 Introduction

Building on decades of modeling advances at the Geophysical Fluid Dynamics Laboratory (GFDL), the System for High-resolution modeling for Earth-to-Local Domains (SHiELD) (Harris et al., 2020) is being progressively extended toward a complete Earth System configuration. A first step in this effort, described in Mouallem et al. (2025), established the atmosphere-ocean coupling framework by integrating SHiELD and MOM6 through the Flexible Modeling System (FMS) full coupler infrastructure. That work demonstrated the technical viability of the coupling strategy using both idealized hurricane simulations and a realistic simulation of Hurricane Helene validating two-way high resolution air-sea interactions in regional domains. In that framework, land processes remained embedded in the atmospheric physics suite and were explicitly identified as a target for future development.

https://doi.org/10.5194/egusphere-2026-2014
Preprint. Discussion started: 19 May 2026

The present work addresses this limitation by introducing GFDL's Land Model version 4 (LM4) into SHiELD as an independent, fully coupled earth system component, thereby completing the transition from a regional coupled atmosphere-ocean to a full global atmosphere-ocean-ice-land model. This is a non-trivial undertaking, LM4 was designed for implicit surface flux coupling within GFDL's modeling infrastructure, while SHiELD employs an explicit atmospheric physics solver. Achieving physically consistent land–atmosphere coupling therefore required a substantial refactoring of the atmospheric physics suite and model drivers, enabling an implicit coupling strategy for both land and ice components withing the established FMS coupler framework.

This integration brings qualitatively new capabilities. Unlike the simplified land representations previously embedded in SHiELD's physics package, LM4 provides a comprehensive treatment of soil hydrology across multiple layers with explicit subsurface water flow, freezing and thawing dynamics, surface and subsurface runoff generation, river routing, snow physics, and dynamic vegetation processes. These capabilities are essential for realistically simulating the land surface response to extreme precipitation events, the evolution of soil moisture and its memory on subseasonal timescales, and the feedbacks between land state evolution and atmospheric dynamics. For coupled high-resolution forecasting applications, the inclusion of a prognostic river routing scheme is particularly impactful: it enables the simulation of downstream flood propagation over multi-day timescales following extreme precipitation, a capability entirely absent in the prior configuration.

In parallel, this work advances the SHiELD software architecture through a flexible and modular design that supports multiple coupled configurations from a single source code and executable without recompilation. This "one code, one executable, one workflow" philosophy, consistent with the broader SHiELD development strategy, facilitates controlled experimentation, ensures backward compatibility with prior configurations, and streamlines the path toward operational deployment.

We demonstrate the new system through a fully coupled global simulation of Hurricane Helene's landfall in September 2024. This event provides an exceptionally demanding and scientifically relevant test case: Helene produced catastrophic flooding in Western North Carolina driven by extreme orographic precipitation interacting with steep terrain and rapidly saturating soils, a scenario that simultaneously stresses the atmospheric dynamics, land surface hydrology, and river routing components of the model. The simulation reveals that the coupled system realistically captures rapid soil saturation, localized runoff generation concentrated in the southern Appalachians, and multi-day river flooding.

This work is organized as follows. Section 2 describes the primary model components. Section 3 describes the coupling methodology including physical processes, implicit coupling and code refactoring. Section 4 presents a high-resolution global simulation and examines the land component's response following the landfall of Hurricane Helene in September 2024.

2 Model Primary Components

The main model components are as described in Mouallem et al. (2025), with the addition of GFDL's land model LM4. We briefly introduce these components here.

https://doi.org/10.5194/egusphere-2026-2014
Preprint. Discussion started: 19 May 2026

2.1 LM4 Land component

The land component is GFDL's Land Model version 4 (LM4.0), a comprehensive land surface model designed to simulate the physical, biological, and chemical processes governing land-atmosphere interactions (Zhao et al., 2018; Held et al., 2019). LM4 represents a significant advancement over its predecessors, incorporating detailed treatments of land surface heterogeneity, soil hydrology, river hydrology, snow physics, and carbon cycling. The model simulates soil hydrology using multiple soil layers with explicit representation of subsurface water flow, freezing and thawing processes. LM4 also incorporates a dynamic vegetation component that captures the evolution of surface and vegetation properties (e.g. leaf area index, biomasses, height, surface roughness), processes (e.g. photosynthesis, transpiration and vertically-resolved water uptake from soil, interception of precipitation) and their responses to climate variability, making it particularly well-suited for long-term climate and earth system modeling applications.

For the purposes of short-term high-resolution prediction modeling explored here, the hydrological and snow modeling capabilities are of most interest. Therefore, biogeochemical cycling and vegetation dynamics are disabled for efficiency and simplicity. However, all LM4 capabilities are available within SHiELD for activation when a scientific need arises.

2.2 SHiELD Atmosphere component

The atmospheric component is the System for High-resolution modeling for Earth-to-Local Domain (SHiELD) (Harris et al., 2020), a nonhydrostatic model using the GFDL Finite-Volume Cubed-Sphere Dynamical Core FV3 (Lin and Rood, 1996, 1997; Lin, 2004; Putman and Lin, 2007; Harris and Lin, 2013; Chen et al., 2013; Harris et al., 2016; Mouallem et al., 2022, 2023; F. Santos et al., 2025) and heavily upgraded physics parameterizations, originally adopted from the Global Forecast System (GFS). Currently, we use the GFDL microphysics scheme version 3 (Zhou et al., 2022b), the Eddy-Diffusivity Mass-Flux (EDMF) boundary layer scheme (Han and Bretherton, 2019), and the scale-aware Simplified Arakawa-Schubert (SAS) convection scheme (Han et al., 2017). For the standalone uncoupled SHiELD configuration, we use the Noah Land Surface Model (Ek et al., 2003) or Noah-MultiParametrization (Niu et al., 2011) and a modified version of the Mixed Layer Ocean of Pollard et al. (1973).

2.3 MOM6-SIS2 Ocean and sea ice component

The ocean and sea ice components employ the Modular Ocean Model version 6 (MOM6) and the Sea Ice Simulator version 2 (SIS2), developed at GFDL (Adcroft et al., 2019). MOM6 employs a finite-volume approach on a C-grid, enabling conservation of mass, heat, and tracers while allowing for flexibility in resolving complex oceanic features, such as boundary currents, mesoscale eddies, and thermohaline circulations. MOM6 is highly configurable, supporting applications ranging from idealized studies to high-resolution global simulations and earth system models. SIS2 complements MOM6 by simulating the dynamics and thermodynamics of sea ice, including ice growth, melt, deformation, and ridging processes. It incorporates advanced parameterizations to capture the essential feedback mechanisms between sea ice, ocean circulation, and atmospheric forcing. The details of ocean configuration follow that of SPEAR-HI and will not be repeated here for brevity.

https://doi.org/10.5194/egusphere-2026-2014
Preprint. Discussion started: 19 May 2026

2.4 FMS Infrastructure layer

The Flexible Modeling System (FMS) (Balaji, 2012; Balaji and Langenhorst, 2012) serves as the infrastructure layer underlying GFDL models. It provides a software environment designed for the efficient development, construction, and execution of atmospheric, oceanic, and climate models written in Fortran (and now DSL and python) for high-performance computing systems. FMS includes MPI domain decomposition for scalable parallel computations, standardized interfaces between component models, and tools for I/O, time-stepping orchestration, and data exchange between model grids. By insulating users from machine-specific details and supporting both distributed and shared memory architectures, FMS enables scientific groups to simultaneously develop new physics and algorithms within a coordinated and collaborative framework.

3 Coupling methodology

3.1 Physical processes

As described in Mouallem et al. (2025), any variable or parameter can be projected between the native grids of a model component and the exchange grid. In the present configuration, a set of dynamic and physical variables from the atmosphere, land and ocean components are mapped onto the exchange grid (called Xgrid thereafter for brevity) where interface quantities are computed and then projected back to each component as shown in figure 1. The general exchange between the ocean, atmosphere and the Xgrid follows that described in Mouallem et al. (2025). Here we additionally include the land component in the exchange workflow to obtain a fully coupled atmosphere-ocean-land model. Atmospheric state variables and radiative fluxes are first projected onto Xgrid, as well as land and ocean surface properties to compute surface fluxes of momentum, heat, and moisture. These fluxes are then mapped back to the corresponding component grids to update their surface boundary conditions. Variables highlighted in green denote the subset of atmospheric variables required to support implicit coupling with the land component. These fields enable a consistent formulation of surface exchange variables to solve the vertical diffusion equation (in the atmosphere mostly eddy diffusivity from the planetary boundary layer scheme) and tendencies for land-atmosphere implicit coupling. This is described in the next section.

https://doi.org/10.5194/egusphere-2026-2014
Preprint. Discussion started: 19 May 2026

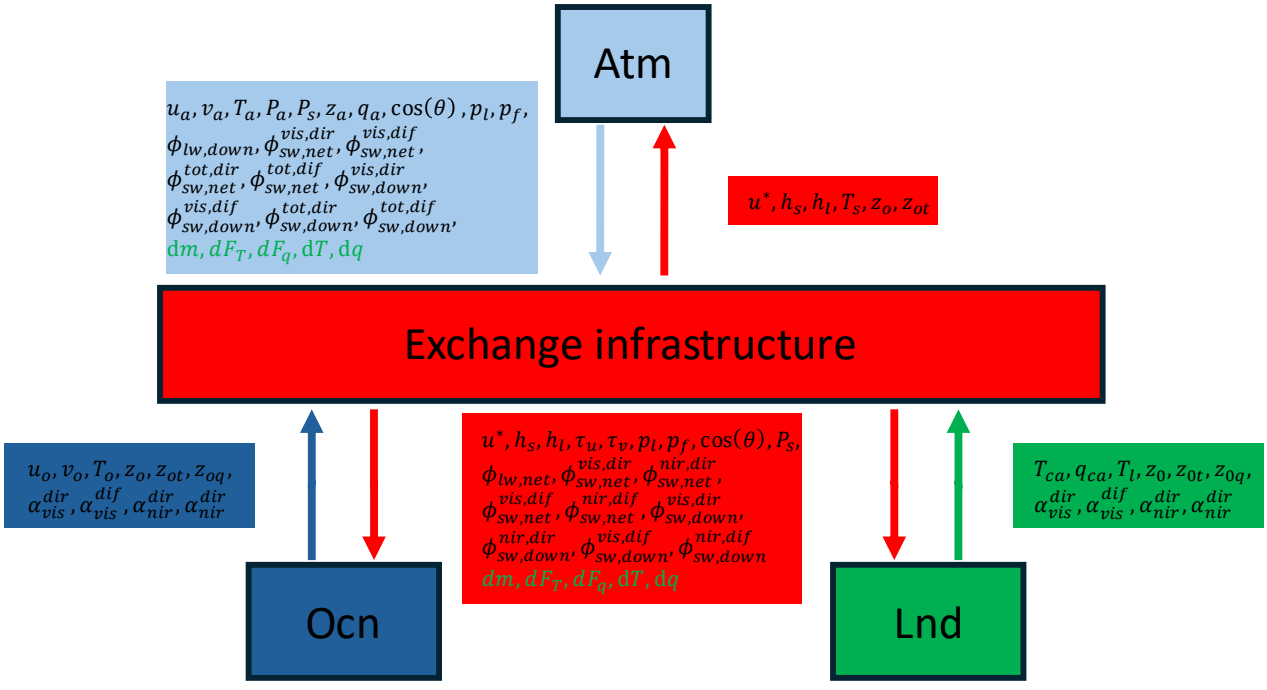

Figure 1. Key variables exchanged through the atmosphere, exchange grid, ocean (including sea ice) and land components. Variables are described in tables 1 and 2

Tables 1 and 2 details the atmosphere and land related variables projected onto the exchange grid shown in figure 1. Atmospheric variables are grouped into two categories: dycore variables, comprising the lowest-level wind components, surface pressure, temperature, layer height, and tracer fields (if present); and physics variables, comprising shortwave and longwave radiation fluxes, liquid and frozen precipitation rates, and the cosine of the solar zenith angle. Land variables include surface parameters such as radiative and canopy air temperature, surface specific humidity, albedo for direct and diffuse shortwave fluxes, and roughness length scales for momentum, heat, and moisture.

https://doi.org/10.5194/egusphere-2026-2014
Preprint. Discussion started: 19 May 2026

Table 1: Summary of the key atmosphere and land variables projected onto the Xgrid. Atmosphere variables are categorized into dynamic variables (output from the FV3 dynamical core) and physics variables (surface-level outputs from the physics suite).

Symbol	Code Variable	Meaning	Units
Variables from FV3 ⇒ Xgrid			
u_a	u_bot	Lowest level wind - zonal component	$m \cdot s^{-1}$
v_a	v_bot	Lowest level wind - meridional component	$m \cdot s^{-1}$
T_a	t_bot	Lowest level temperature	K
P_a	p_bot	Lowest level pressure	Pa
P_s	p_s	Surface pressure	Pa
q_a	tr_bot	Lowest level specific humidity	-
z_a	z_bot	Height for the lowest layer	m
Surface Variables from SHiELD Physics ⇒ Xgrid			
$\cos(\theta)$	coszen	Cosine of the solar zenith angle	-
p_l	lprec	Liquid precipitation rate	$kg \cdot m^{-2} \cdot s^{-1}$
p_f	fprec	Frozen precipitation rate	$kg \cdot m^{-2} \cdot s^{-1}$
$\phi_{lw,down}$	flux_lw	Downward longwave flux	$W \cdot m^{-2}$
$\phi_{sw,net}^{vis,dir}$	flux_sw_vis_dir	Net (upward - downward) direct visible shortwave flux	$W \cdot m^{-2}$
$\phi_{sw,net}^{vis,dif}$	flux_sw_vis_dif	Net (upward - downward) diffuse visible shortwave flux	$W \cdot m^{-2}$
$\phi_{sw,net}^{tot,dir}$	flux_sw_dir	Net (upward - downward) direct total shortwave flux	$W \cdot m^{-2}$
$\phi_{sw,net}^{tot,dif}$	flux_sw_dif	Net (upward - downward) diffuse total shortwave flux	$W \cdot m^{-2}$
$\phi_{sw,down}^{vis,dir}$	flux_sw_down_vis_dir	Downward direct visible shortwave flux	$W \cdot m^{-2}$
$\phi_{sw,down}^{vis,dif}$	flux_sw_down_vis_dif	Downward diffused visible shortwave flux	$W \cdot m^{-2}$
$\phi_{sw,down}^{tot,dir}$	flux_sw_down_total_dir	Downward direct total shortwave flux	$W \cdot m^{-2}$
$\phi_{sw,down}^{tot,dif}$	flux_sw_down_total_dif	Downward diffused total shortwave flux	$W \cdot m^{-2}$
Land variables ⇒ Xgrid			
T_{ca}	t_ca	Canopy temperature	K
q_{ca}	q_ca	Canopy specific humidity	-
T_l	t_surf	Land surface (radiative) temperature	K
z_0	rough_mom	Roughness length for momentum	m
z_{0t}	rough_heat	Roughness length for heat	m
z_{0q}	rough_moist	Roughness length for moisture	m

Continued on next page

https://doi.org/10.5194/egusphere-2026-2014
Preprint. Discussion started: 19 May 2026

Symbol	Code Variable	Meaning	Units
α	`albedo`	Broadband Albedo	-
α_{vis}^{dir}	`albedo_vis_dir`	Albedo for direct visible shortwave flux	-
α_{vis}^{dif}	`albedo_vis_dif`	Albedo for diffuse visible shortwave flux	-
α_{nir}^{dir}	`albedo_nir_dir`	Albedo for direct near-infrared shortwave flux	-
α_{nir}^{dif}	`albedo_nir_dif`	Albedo for diffuse near-infrared shortwave flux	-

Land implicit coupling

Table 2: Summary of additional variables needed for atmosphere and land variables implicit coupling (shown in green in figure 1).

Symbol	Code Variable	Meaning	Units
dm	`dtmass`	Atmosphere timestep divided by lowest atmosphere layer mass	$m^2 \cdot s \cdot kg^{-1}$
dF_T	`dflux_t`	Top of the lowest atmospheric layer heat flux increment	$kg \cdot m^{-2} \cdot s^{-1}$
dF_q	`dflux_q`	Top of the lowest atmospheric layer moisture flux increment	$kg \cdot m^{-2} \cdot s^{-1}$
dT	`delta_t`	Top of the lowest atmospheric layer temperature increment	K
dq	`delta_tr`	Top of the lowest atmospheric layer moisture increment	$kg \cdot kg^{-1}$

Figure 2 presents a schematic representation of two alternative coupling strategies employed to solve the vertical diffusion equation across the land–atmosphere interface. In both panels, the vertical discretization is depicted as a series of horizontal layers indexed by k, with the land surface prescribed as the lower boundary condition.

The explicit coupling scheme (left panel) employs a sequential approach. Here, the atmospheric vertical diffusion, computed implicit-in-time to ensure numerical stability, results in a tridiagonal matrix which is solved first (Arrows 1), typically using surface fluxes (heat, moisture) calculated from the state of the land surface at the previous time step (t). The tridiagonal solver performs both its downward and upward sweeps independently of the current land surface update. Next, the land surface model advances its state (Arrows 2) using the updated lowest layer atmospheric variables as forcing. In this process, the canopy or first soil layer is updated first (first small arrow in Arrow 2), followed by the soil heat diffusion solver, and then the canopy temperature is updated again. In the explicit scheme, the lagging of the lower boundary condition decouples the mathematical solution of the turbulent transport between land and atmosphere, which can introduce inconsistencies between the surface fluxes and the atmospheric state, potentially degrading numerical stability at longer time steps.

On the other hand, the implicit scheme avoids this inconsistency by integrating the land surface directly in the atmospheric tridiagonal solver as a single extended column. The atmospheric downward sweep proceeds from the top of the atmosphere to the land surface (Arrow 1), at which point the land surface solver is invoked (Arrow 2). Consequently, the the relationship be-

https://doi.org/10.5194/egusphere-2026-2014
Preprint. Discussion started: 19 May 2026

tween surface fluxes and land surface is linearized and the lowest atmosphere layer and land surface are solved simultaneously. Finally, the atmosphere upward sweep propagates from the updated surface to the top of the atmosphere (Arrow 3). It is worth mentioning that implicit coupling also applies to the ice component which is advanced in the fast loop of the solver as shown later. The ocean will stay explicitly coupled to the atmosphere.

This implicit strategy maintains consistency between surface fluxes and turbulent transport, improving numerical stability and conservation within a single time step. This approach is applied only to temperature and moisture in the current implementation. The same could be done for momentum and other tracers; however, we assume that surface fluxes of momentum and other tracers have no implicit dependence on surface parameters. Implicit momentum coupling may become important in future implementation for higher resolution configurations.

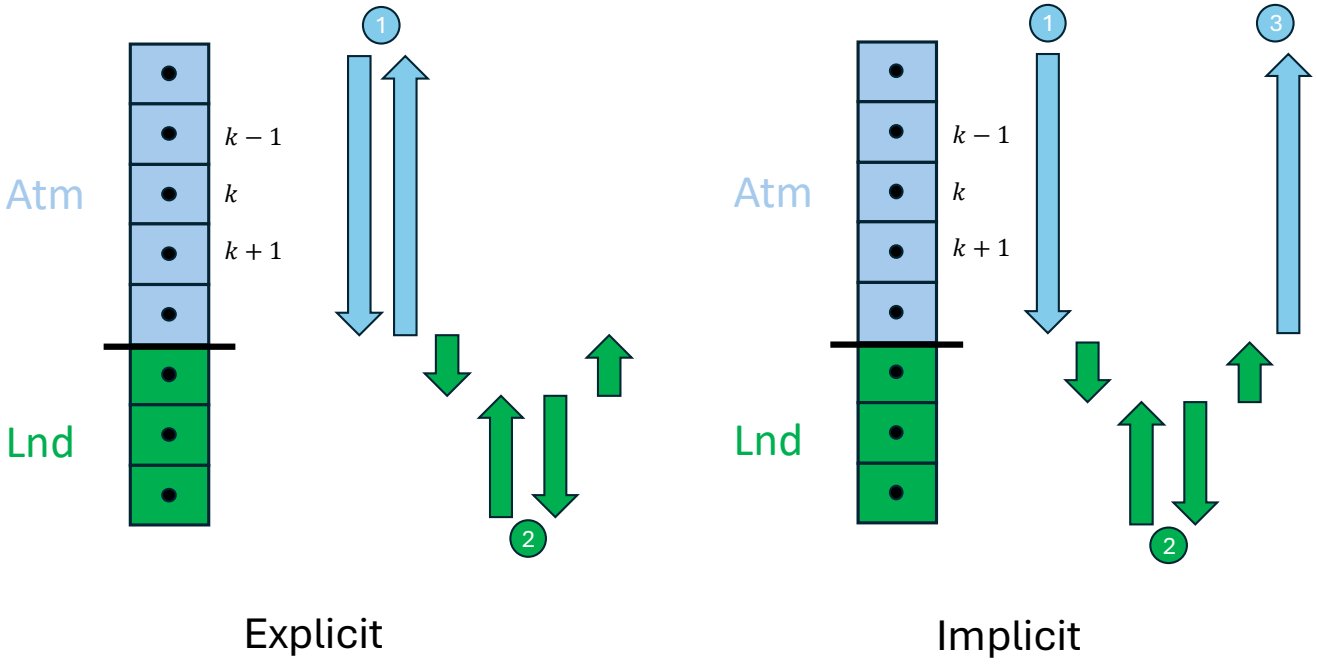

Figure 2. Schematic of explicit (left) and implicit (right) coupling schemes for vertical diffusion across the land–atmosphere interface. Arrows indicate the sequence of atmospheric and land surface tridiagonal solver sweeps within a single time step.

3.2 Software framework and code refactoring

Figure 3 illustrates a schematic of a 1D exchange grid for a full atmosphere, ocean and land coupled model. Analogous to the projection of near-surface atmospheric and oceanic state variables onto the Xgrid in Mouallem et al. (2025), land surface variables and parameters are now likewise projected onto the exchange grid. On the Xgrid, surface fluxes of momentum, heat, moisture, and radiation are diagnosed using land-specific surface properties (e.g., roughness lengths, albedo, and surface

https://doi.org/10.5194/egusphere-2026-2014
Preprint. Discussion started: 19 May 2026

temperature and humidity) and are subsequently remapped to the atmosphere and land component grids. This extension allows the land–atmosphere interface to be treated consistently with the ocean–atmosphere interface, while maintaining the same conservative and modular coupling strategy. The coupling frequency remains user-configurable and subject to the constraints discussed in Part I.

An important feature illustrated in Figure 3 is that a single atmospheric grid cell can geometrically overlap both the land and ocean grids, as shown by the vertical dashed lines. In such cases, the atmospheric grid cell is associated with multiple exchange grid cells, each corresponding to the area of intersections between atmospheric cells with the land and ocean component grid cells (Balaji et al., 2006). On the land and sea ice side, the Xgrid cells can be further subdivided dynamically to represent inherent heterogeneity of the surface, such as area fractions of lakes, glaciers, croplands, and forests in the land grids, and different thickness categories of the sea ice. All flux computations are performed on this Xgrid representation. Since surface fluxes from the land and ocean depend nonlinearly on the atmosphere and surface properties, they are evaluated independently over their respective Xgrid areas and are subsequently area-averaged when remapped to the atmospheric grid. Similarly, atmospheric fields are consistently distributed to the land and ocean components according to the same geometric decomposition. This prevents or greatly minimizes numerical discontinuities between different components at the coastlines.

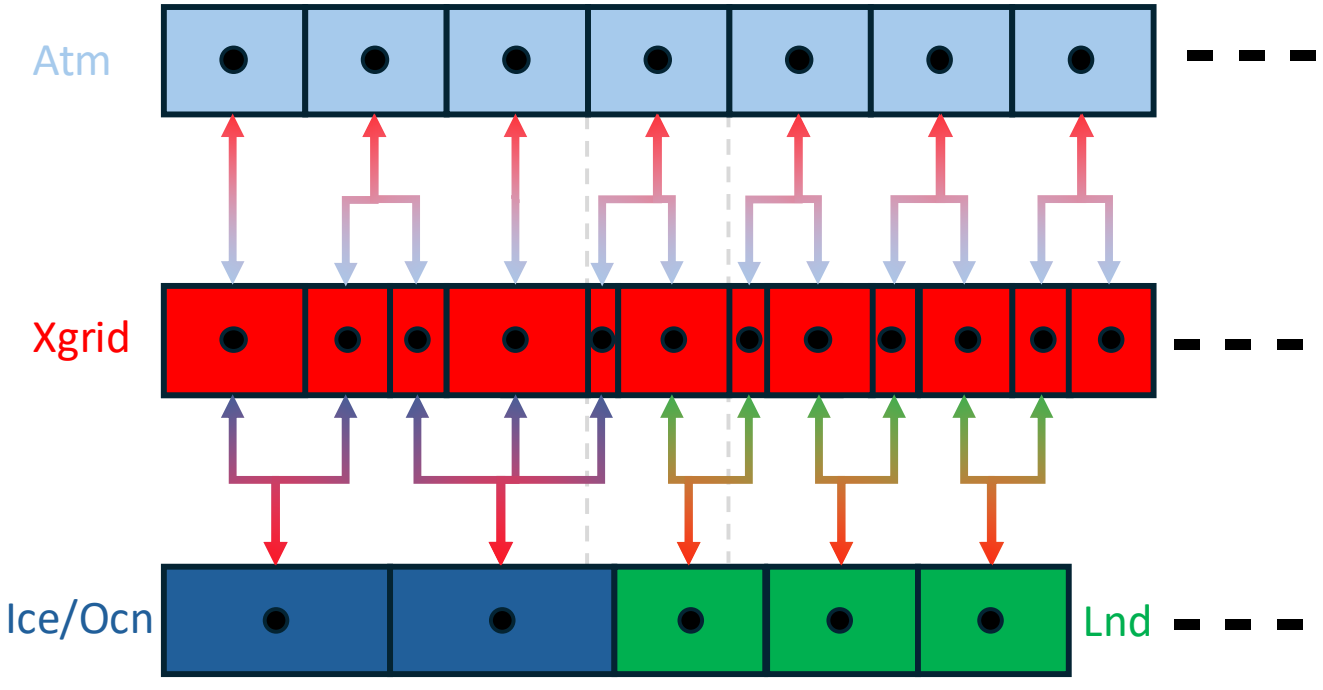

Figure 3. Schematic of a one-dimensional exchange grid and communication map between the atmosphere, land and ice components at different resolutions. The red side of the arrow indicate where variables are projected from the exchange grid. The light-blue, dark blue and green sides of the arrow represent the projection of variables to the exchange grid from the atmosphere, ice or land components, respectively.

https://doi.org/10.5194/egusphere-2026-2014
Preprint. Discussion started: 19 May 2026

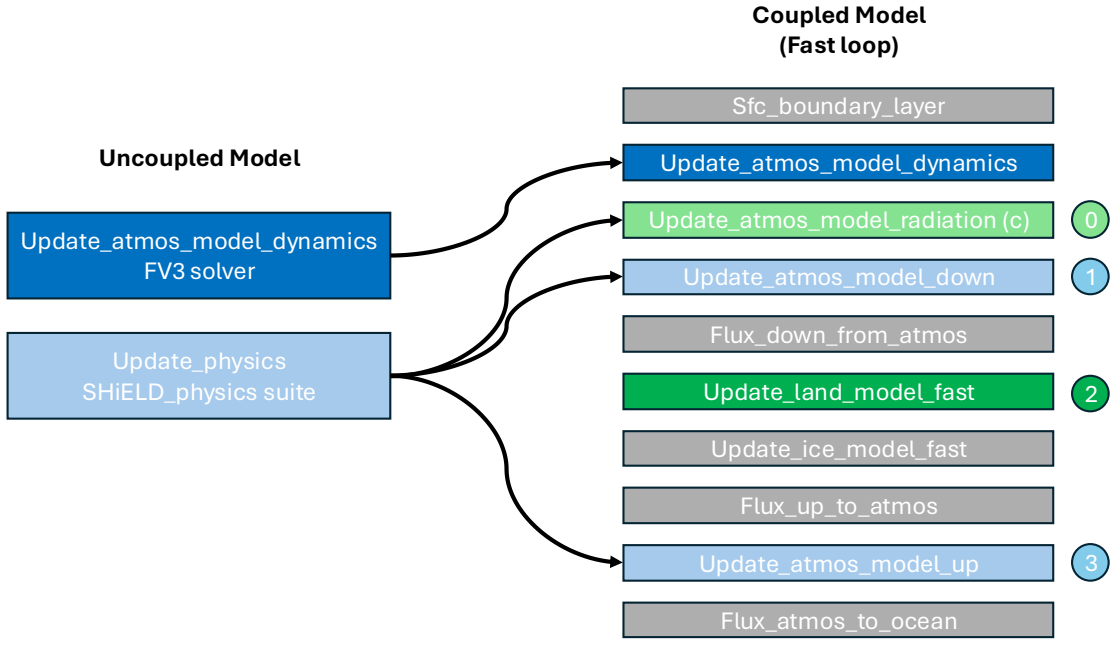

Figure 4. Schematic of the code structure of the uncoupled and coupled models. Arrows show the uncoupled components that are refactored in the coupled call sequence.

Figure 4 illustrates the structural refactoring of the model required to transition from the uncoupled configuration to the coupled model's 'fast loop' of the FMS full coupler. The left panel depicts the legacy uncoupled model which encapsulates the time-stepping into two primary high level drivers:

- Dynamics: update the dynamics using the dynamical core FV3
- Physics: compute the physics tendencies from SHiELD's physics parameterization suite

The right panel details the fast loop of the coupled model, demonstrating how the monolithic calls are decomposed and re-ordered to facilitate tighter coupling between different model components. As indicated by the arrows, the dynamics component maps directly to the dynamic update call within the coupled sequence. The physics component is split into three distinct phases (0-1-3) allowing tighter coupling with land and ice. The execution sequence proceeds as follows:

- `Sfc_boundary_layer`: compute explicit fluxes and their derivatives at the surface boundary
- `Update_atmos_model_dynamics`: update the dynamics using the dynamical core FV3
- `Update_atmos_model_radiation`: compute radiation tendencies

https://doi.org/10.5194/egusphere-2026-2014
Preprint. Discussion started: 19 May 2026

- `Update_atmos_model_down` calculate the necessary atmospheric states to drive surface processes. This is where the downward sweep of heat and moisture is computed for implicit coupling.
- `Flux_down_from_atmos`: compute fluxes and derivatives corrected for implicit coupling.
- `Update_land_model_fast`: perform the land model fast time integration loop
- `Update_ice_model_fast`: perform the ice model fast time integration loop
- `Flux_up_to_atmos`: correct the flux given the updates land and ice variables
- `Update_atmos_model_up`: perform the upward sweep of the heat and moisture and all the remaining physics updates.
- `Flux_atmos_to_ocean`: correct fluxes of some fields to be passed to the ocean.

Figure 5 illustrates the code structure for the uncoupled and coupled models. In the uncoupled model, the dynamics are called first for a timestep dt_atmos. The updated solution is then passed to the physics paramterizations where all physics tendencies are computed and used later on to update the model state. As implied by the schematic, all the physics parameterization are computed, in-bulk at this stage including:

1. Surface layer and surface energy balance (over land, ocean, and sea-ice), including turbulent exchange coefficients, near-surface diagnostics, and land/sea-ice model updates.
2. Planetary boundary layer (PBL) vertical mixing, providing turbulent transport of momentum, heat, moisture and other tracers.
3. Orographic and convective gravity-wave drag as well as Rayleigh damping, which modify momentum and temperature.
4. Radiative heating (shortwave and longwave), passed from the radiation scheme and applied at the physics timestep.
5. Ozone and stratospheric water-vapor chemistry tendencies.
6. Shallow and deep convection(based on mass-flux parameterizations), including convective heating, transport and detrainment of tracers, and convective precipitation.
7. Cloud microphysics, including large-scale condensation/evaporation and precipitation processes.
8. Diagnostic routines, including precipitation type, land-surface adjustments, and calculation of precipitation, cloud fraction, cloud water/ice, and near-surface fields.

https://doi.org/10.5194/egusphere-2026-2014
Preprint. Discussion started: 19 May 2026

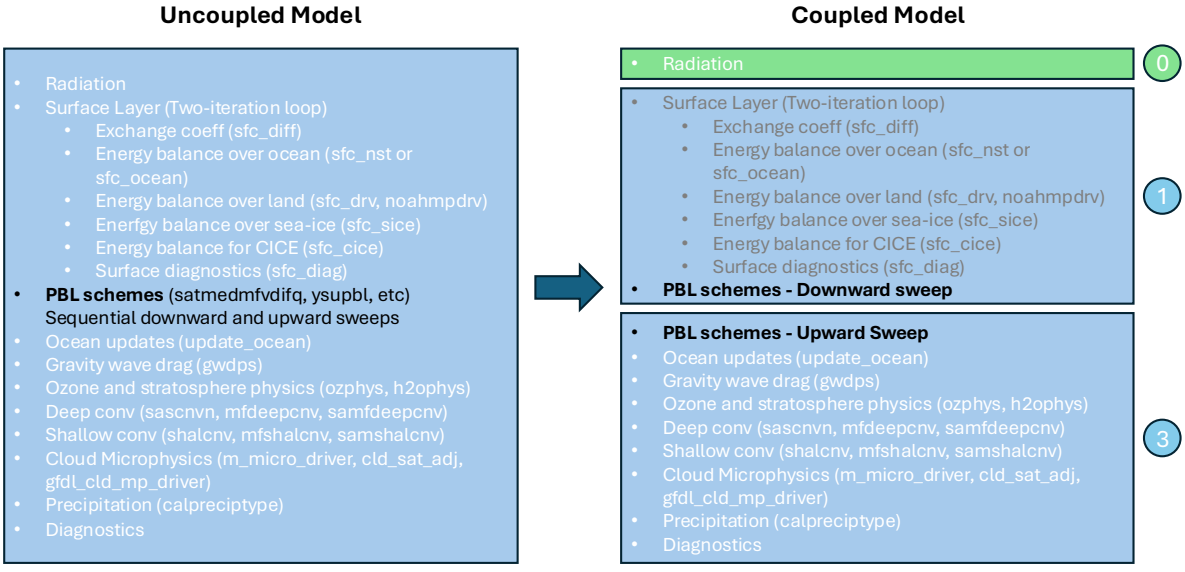

Figure 5. Schematic of the time-integration sequence in the uncoupled (left) and coupled (right) SHiELD configurations. The arrows highlight the refactored structure of the physics suite. Grey text denotes the SHiELD_physics surface layer flux computation, which is enabled in the uncoupled configurations and disabled for the coupled configurations.

Figure 5 also details the internal restructuring of the physics suite required to support the coupled configuration including land implicit coupling. The refactoring process consists of splitting this monolithic structure into different components as described in figure 4 to have a radiation module, a surface and downward physics step and lastly, and upward and moist processes step. The right panel illustrates the new refactored structure. Radiation routines (step 0) are now split and called separately. Step (1) corresponding to `Update_atmos_model_down` contains the uncoupled surface flux calculations, the downward sweep of the tridiagonal matrix for heat and moisture. Step (3) corresponding to `Update_atmos_model_up` contains the remaining physics calls. It is important to note that the momentum and the turbulent kinetic energy (TKE) upward and downward sweep are still explicit in `Update_atmos_model_down`.

3.3 Flexible Surface-Coupling Architecture and Surface Flux Pathways

It is important to make the distinction between the surface layer calculation in `sfc_boundary_layer` shown in figure 4 and those shown as a grey text in figure 5. The former represents surface fluxes at the coupler level, computed on the Xgrid between the atmosphere and ice/ocean components, as well as between the atmosphere and land components. In contrast, the later surface layer calculation in `update_atmos_model_down` correspond to fluxes produced internally by the atmospheric

https://doi.org/10.5194/egusphere-2026-2014
Preprint. Discussion started: 19 May 2026

physics when interacting with embedded surface representation, such as the mixed-layer ocean and the NOAH or NOAH-MP land models. These internal flux computations are enabled for uncoupled model configurations and disabled for coupled configurations through Xgrid.

The current framework allows running different model configurations from a single source code and executable, without requiring recompilation. Following the "one code, one executable, one workflow" design philosophy, figure 6 illustrates the flexible surface-coupling software architecture allowing different coupled configurations to be set up from a common set of model components. The configurations differ in the complexity of their surface boundary components and the pathways of surface fluxes. The baseline uncoupled SHiELD configuration couples FV3–SHiELD_physics to null ocean and null land/ice components, providing a simple atmosphere-only (simple land and ocean are embedded in the physics) framework bypassing the exchange grid infrastructure. The SHiELD-MOM6 configuration replaces the null ocean/ice components with the MOM6/SIS2 ocean and sea-ice models, enabling two-way atmosphere–ocean–ice coupling while retaining a null land component. The SHiELD-LM4 configuration introduces the LM4 land model in place of the null land component but retains null ocean and ice components, allowing for interactive land–atmosphere coupling without a dynamic ocean. Finally, the SHiELD-MOM6-LM4 configuration is the most complete, coupling FV3–SHiELD_physics simultaneously to MOM6, SIS2, and LM4, thus representing a fully coupled atmosphere–ocean–sea ice–land system. The three later configurations will invoke the exchange grid infrastructure. This modular architecture enables seamless switching between configurations via runtime namelist settings, without requiring recompilation of a new executable. In this context, it is worth elaborating on the null components. The null components act as passive placeholders that enable consistent coupling infrastructure without introducing additional physics or state evolution. Their primary role is to satisfy the interface requirement of the full coupler when a given component is absent or deactivated, by providing dummy routines and state variables necessary for the full model compilation and execution.

https://doi.org/10.5194/egusphere-2026-2014
Preprint. Discussion started: 19 May 2026

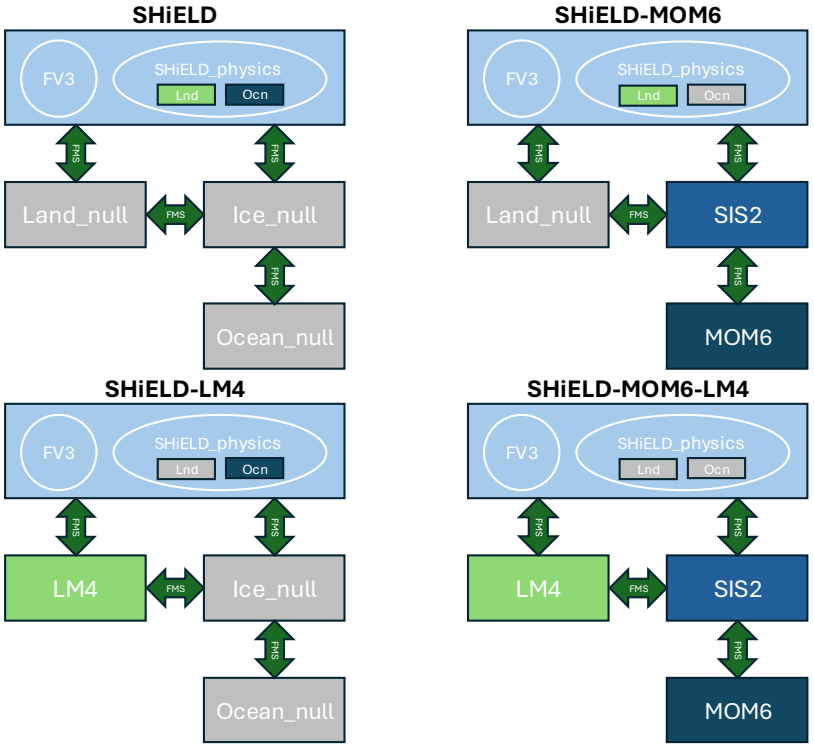

Figure 6. Schematic of different uncoupled and coupled model configurations. Land and ocean grid points are updated either by simplified surface schemes within the SHiELD physics suite or by fully interactive component models (e.g., MOM6 or LM4) coupled through the FMS coupler.

4 Simulations

We perform fully coupled global simulations using the SHiELD-MOM6-LM4 modeling system as presented in figure 6. The atmospheric component is the SHiELD v2022 configuration (Zhou et al., 2022a, b) which uses a C768 cubed-sphere grid, corresponding to a quasi-uniform horizontal resolution of approximately 13km. The land model configuration, adopted from SPEAR-HI (Delworth et al., 2020), is using a C384 grid, corresponding to a global resolution of roughly 25km. Given that we are focusing on the land model response and the hurricane is initialized right when it hits the coast with minor atmosphere-ocean interaction, we employ a coarse resolution one-degree ocean configuration on the tripolar grid with grid refinement to 1/3 degree near the Equator, also from SPEAR. Atmospheric initial conditions are taken from the GFS analysis at 00:00Z on 27 September 2024, immediately prior to the landfall of Hurricane Helene. The land and ocean initial conditions are taken from September 1 2024 model output where the model was previously forced using SSP2-4.5 (O'Neill et al., 2016; van Vuuren et al., 2014) scenario radiative forcings.

The fully coupled SHiELD-MOM6-LM4 system is integrated for three days. In this configuration, surface fluxes exchanged between the atmosphere, land, and ocean are computed and passed exclusively through the full FMS coupler. As a result, the

https://doi.org/10.5194/egusphere-2026-2014
Preprint. Discussion started: 19 May 2026

atmospheric model receives land and ocean surface fluxes from the coupled land and ocean components, rather than from the internal parameterizations in the SHiELD physics suite (SHiELD_physics), and vice versa. This is described in section 3. The primary objective of these simulations is to evaluate the land coupling framework and evaluate the land component response to atmosphere forcing.

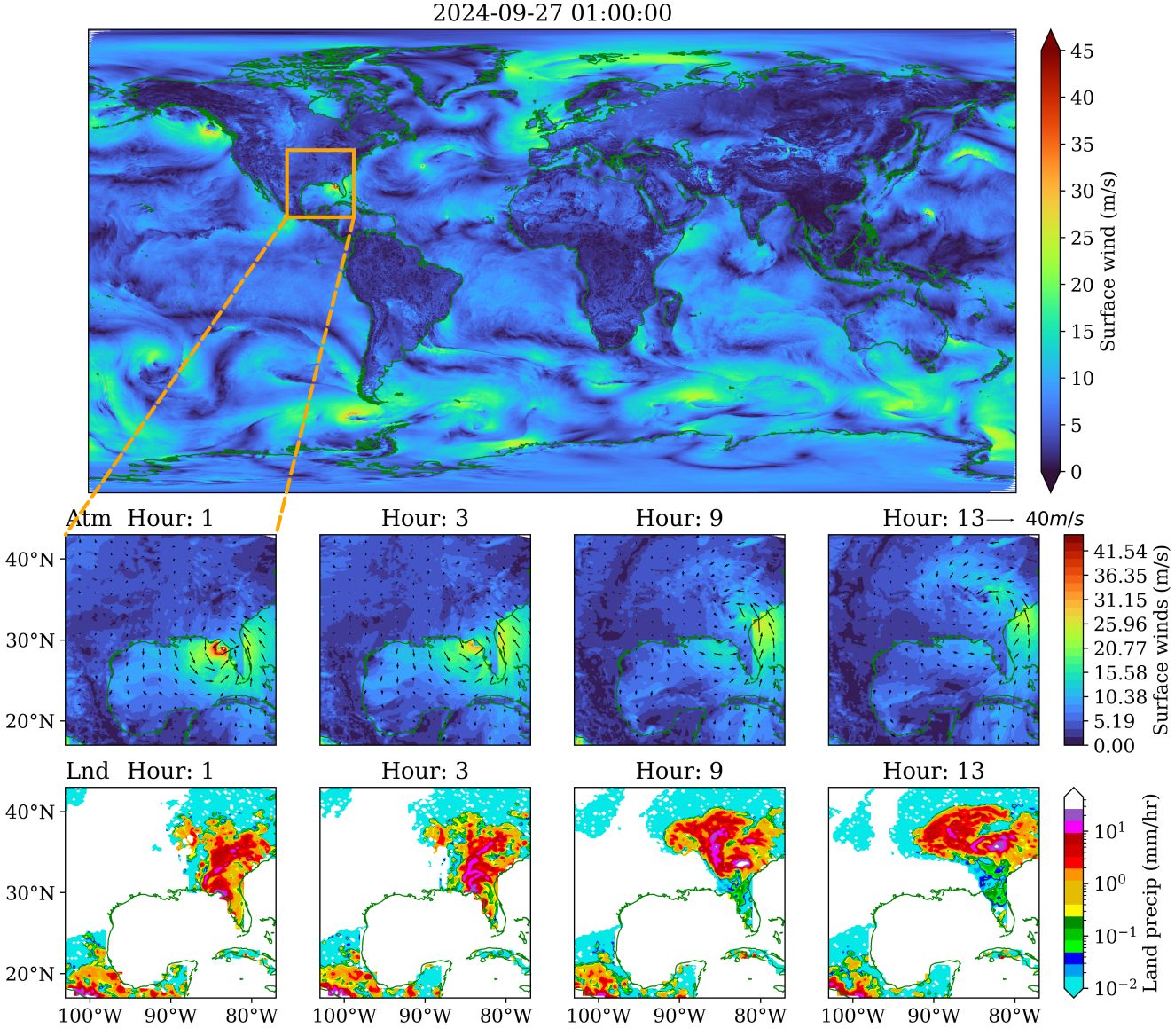

Figure 7. Global surface wind speed (top row) and regional time evolution of atmospheric surface winds (middle row) and precipitation seen by the land component (bottom row) over the southeastern United States and Gulf of America for hours 1, 3, 9 and 13. The orange box indicates the zoomed in region. Black arrows denote the local near-surface wind velocity vectors.

https://doi.org/10.5194/egusphere-2026-2014
Preprint. Discussion started: 19 May 2026

Figure 7 shows surface wind magnitude and vectors from the atmospheric component (middle row) alongside the precipitation field received by the land component (bottom row) at hours 1, 3, 9, and 13 of the simulation. The atmospheric surface winds (middle row) clearly capture the storm's cyclonic circulation, with peak wind speeds exceeding 40 m/s concentrated in the eyewall region near the Gulf Coast at hour 1, consistent with major hurricane intensity. The characteristic asymmetric wind structure of a landfalling hurricane is evident, with the right-of-track quadrant exhibiting the strongest winds due to the superposition of the storm's rotational winds and its translational velocity. As the storm progresses through hours 3 to 13, the surface wind field shows progressive weakening over land, reflecting the increased surface roughness and reduced moisture supply that drive the well-known rapid intensification decay upon landfall. The land precipitation field (bottom row) reveals the spatial coherence between the atmospheric forcing and the land model's received precipitation. The precipitation maximum tracks consistently with the storm's wind circulation center, and the spiral rainband structure visible in both fields confirms that the atmosphere-land coupling is transmitting the storm's mesoscale organization faithfully across the component interface to the land component. The progressive inland penetration of precipitation from hours 1 to 13 demonstrates that the land model receives a physically consistent and temporally continuous forcing through the coupling layer.

https://doi.org/10.5194/egusphere-2026-2014
Preprint. Discussion started: 19 May 2026

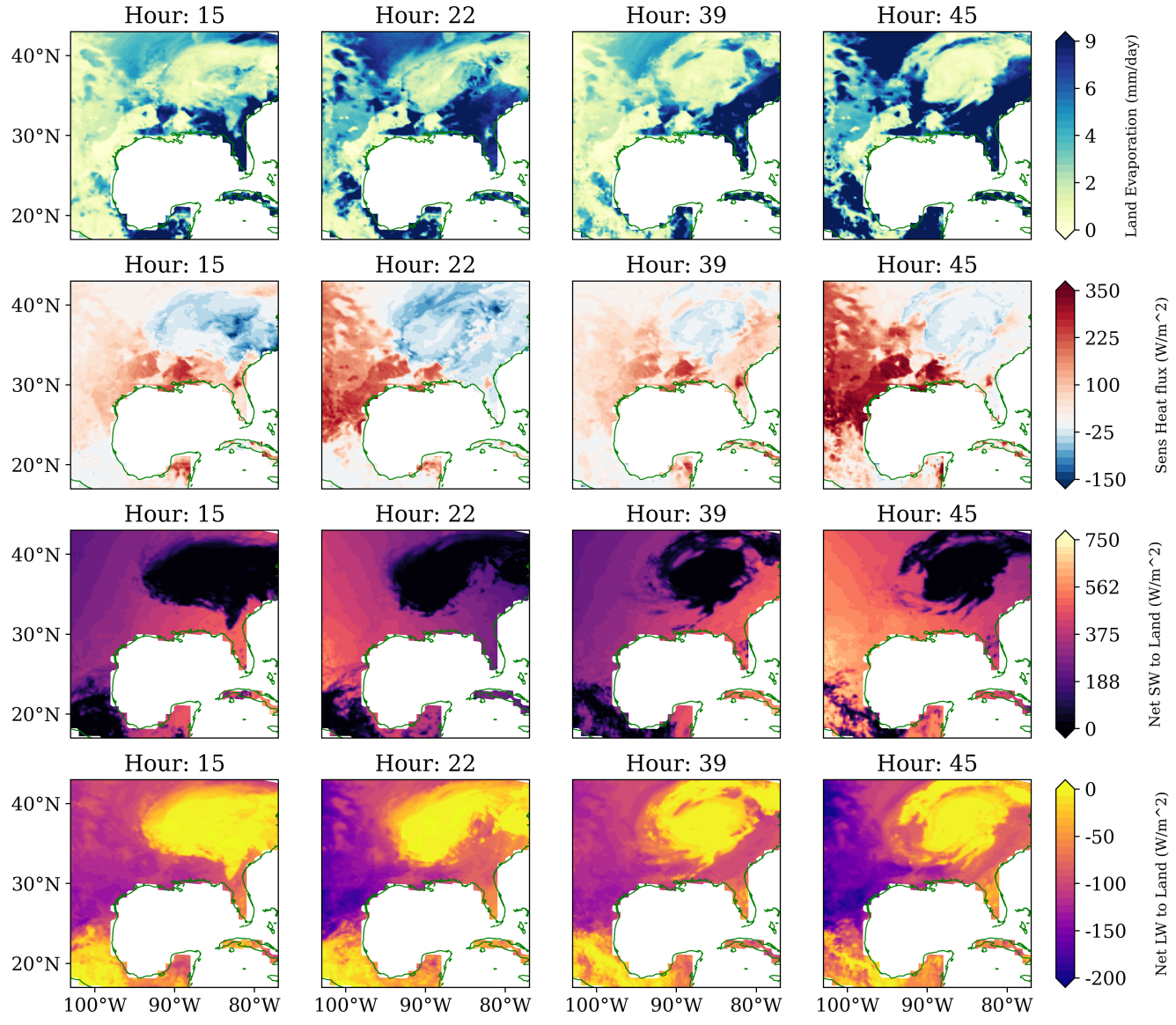

Figure 8. Two-dimensional snapshots of the time evolution of selected diagnostics from the land component: land evaporation (row 1), sensible heat flux (row 2), net shortwave radiation (row 3), and net longwave radiation (row 4) for hours 15, 22, 39 and 45.

Figure 8 show the evolution of several instantaneous surface fluxes as diagnosed by the land component. The panels depict land evaporation, sensible heat flux, net shortwave radiation and net longwave radiation at hours 15, 22, 39 and 45 and spanning inland throughout the storm progression. Land evaporation displays reduced values beneath persistent heavy rainfall and hurricane clouds and enhanced fluxes once the storm passes. The spatial pattern clearly reflects this competing behavior as expected. The sensible heat flux (row 2) exhibits a pronounced negative anomaly ($-150\,\mathrm{W/m^2}$) collocated with the storm's

https://doi.org/10.5194/egusphere-2026-2014
Preprint. Discussion started: 19 May 2026

spiral bands and eye, indicative of suppressed surface shortwave heating and enhanced surface evaporative cooling under the dense cloud shield and heavy precipitation, while positive values exceeding $350\,\mathrm{W/m^2}$ persist in clear-sky regions surrounding the storm. The net shortwave radiation reaching the land surface (row 3) captures a clear diurnal signal modulated by the storm's cloud cover: these plots show values approaching $750\,\mathrm{W/m^2}$ in cloud-free regions, while the storm shadow imposes near-zero shortwave fluxes beneath the cloud canopy, consistent with the optical thickness of hurricane convective systems.

Net longwave radiation exhibits a response complementary to, and opposite of, the net shortwave radiation. Its values are predominantly negative in the clear sky environment surrounding the storm, where land surface loses longwave radiation freely to the clear atmosphere, while beneath the hurricane's dense clouds the net LW is suppressed toward zero by the downwelling longwave emission from the clouds. The spatial pattern closely follows the cold-core cloud structure, indicating that the model realistically captures the radiative signature of dense clouds. In the outer regions of the storm domain, where cloud cover is warmer and optically thinner, longwave cooling is weaker but remains negative, consistent with a gradual transition from the cloud-free state to the storm's intense core.

Collectively, these diagnostics demonstrate that the land model responds coherently to hurricane forcing, reproducing the expected redistribution of radiative and turbulent energy fluxes across both the storm core and the surrounding environment. The spatial alignment between cloud structure, radiative forcing, and turbulent flux anomalies, as well as their inland displacement with storm progression, indicates dynamically consistent coupling between atmospheric processes and land-surface energetics across the diurnal cycle.

The hydrological response of the land model to Hurricane Helene is examined through complementary diagnostics: soil liquid water content, surface runoff, and river flow with a particular focus on North Carolina which was severely impacted by the storm's catastrophic flooding.

https://doi.org/10.5194/egusphere-2026-2014
Preprint. Discussion started: 19 May 2026

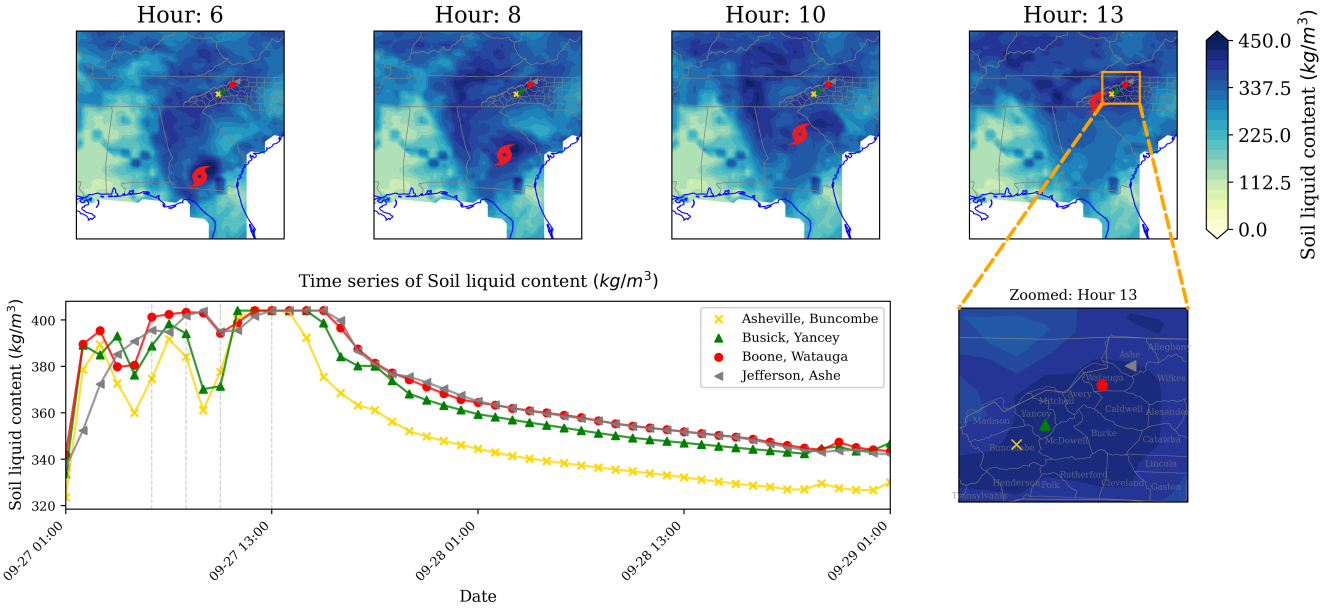

Figure 9. Surface Soil liquid water content of the top soil layer (0.01 m) during Hurricane Helene shown as spatial snapshots at hours 6, 8, 10, and 13 (top), time series at four locations in western North Carolina (bottom left), and a zoomed view of the hour 13 snapshot centered on the western North Carolina region (bottom right). The hurricane symbol indicates the storm's position at each hour. Vertical dashed vertical lines in the time series corresponds to the hours shown in the spatial snapshots.

Figure 9 shows the regional spatial distribution of the soil liquid water content in the top soil layer ($0.01\,\mathrm{m}$). The spatial map already shows a moderate saturated soil which is the typical condition in late September. As the storm moves inland, the soil becomes highly saturated as shown by the dense blue color of the snapshots. The western North Carolina region show a progressive increase toward full saturation between hours 6 and 13, with the Asheville area and surrounding counties reaching maximum values exceeding $400\,\mathrm{kg/m^3}$ by hour 13. In the second row, we consider the time series of soil water content at four different location, severely hit by the storm: Asheville/Buncombe, Busick/Yancey, Boone/Watauga and Jefferson/Ashe. All four locations reach saturation simultaneously at hour 13 but diverge during the post-storm drainage phase. The Asheville/Buncombe location drains most rapidly, likely reflecting differences in soil texture and topographic slope at that grid cell, while the Boone/Watauga and Jefferson/Ashe locations retain elevated soil moisture for longer, suggesting slower drainage. XXX This spatial heterogeneity in the post-storm recovery is physically realistic and highlights the model's sensitivity to local soil and topographic properties. XXXX

https://doi.org/10.5194/egusphere-2026-2014
Preprint. Discussion started: 19 May 2026

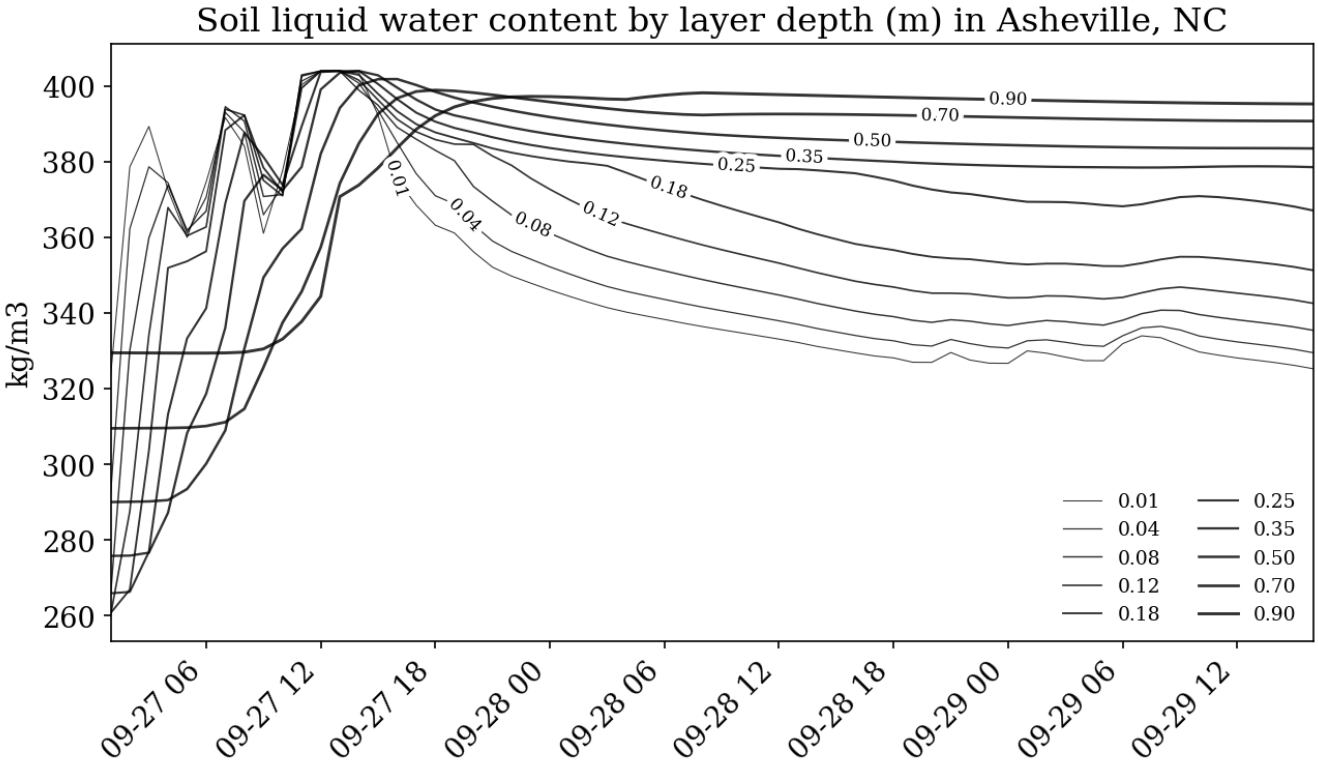

Figure 10. Soil liquid water content (kg/m^3) at the Asheville, Buncombe County grid cell as a function of time during Hurricane Helene, shown for each soil layer depth (m) up to 0.9 m depth.

295 The point time series at Asheville, Buncombe provides a detailed vertical perspective on the soil saturation process as shown in figure 10. Before the storm arrives, soil moisture naturally changes with depth, with different layers showing a typical pattern of variability. As intense storm precipitation reaches the region around 09-27 12Z, all soil layers rapidly converge to saturation at approximately $400\,\mathrm{kg/m^3}$ in a few hours, demonstrating the land model's ability for water to percolate downward through the soil column in response to extreme rainfall. Following saturation, the drainage rate is clearly depth-dependent: in shallow
300 layers (0.01–0.12 m) soil water content decreases relatively quickly as gravitational drainage and surface evaporation deplete near-surface moisture, while deeper layers (0.50–0.90 m) remain near saturation for the remainder of the simulation period. This observed behavior is physically consistent.

https://doi.org/10.5194/egusphere-2026-2014
Preprint. Discussion started: 19 May 2026

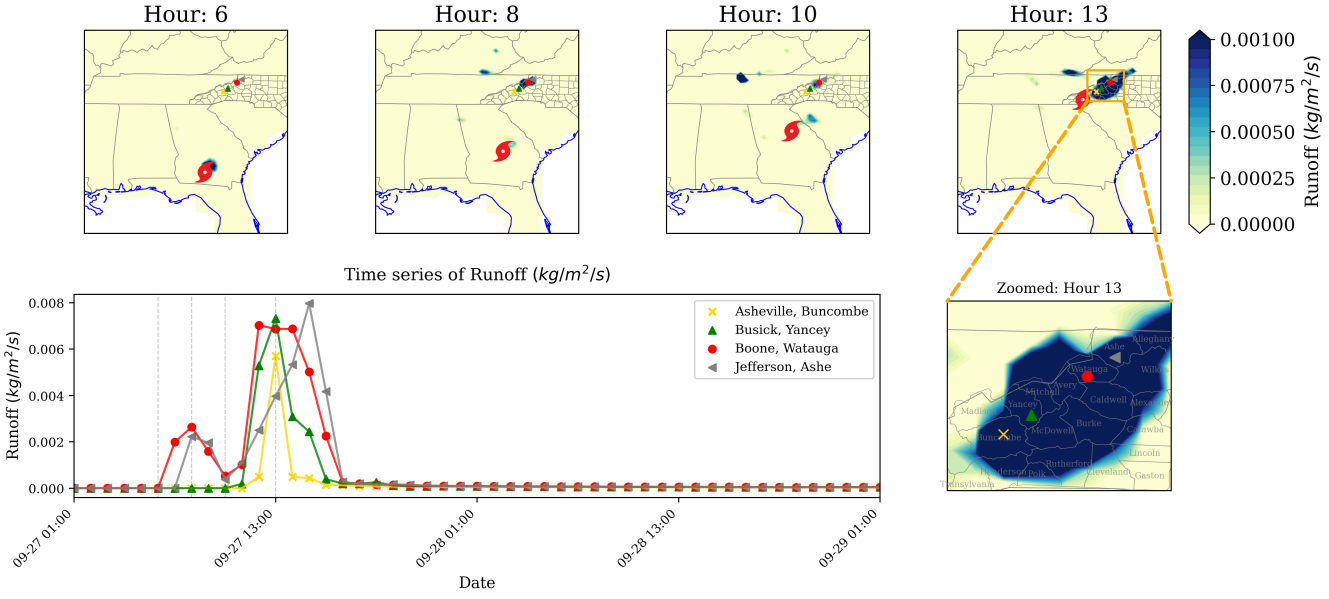

Figure 11. As for figure 9 but for land surface runoff.

Once soil approaches saturation, the dominant hydrological process shifts towards runoff. The runoff response is sharp, localized and dramatic, as seen in figure 11. Prior to the storm the runoff at all four locations is zero, consistent with unsaturated soil able to absorb incoming precipitation. As the storm's precipitation arrives on 09-27, runoff at Boone/Watauga and Busick/Yancey rises sharply to peak values exceeding 0.006–0.007 $\mathrm{kg/m^2/s}$. The peak is extremely brief, lasting a few hours before returning to near-zero values, consistent with the episodic nature of the precipitation forcing. The Jefferson, Ashe location exhibits a slightly delayed and higher runoff peak relative to Boone and Yancey, which may reflect differences in local precipitation intensity or the effect of the already-elevated antecedent soil moisture at that location. The spatial maps confirm that the runoff signal is tightly localized to the southern Appalachians throughout hours 6–13, with the zoomed inset at hour 13 clearly showing the runoff maximum concentrated over the four counties, Buncombe, Yancey, Watauga, Ashe, and surrounding counties. This is precisely the area that experienced catastrophic flash flooding during Hurricane Helene.

The riverflow response, shown in figure 12, completes the hydrological sequence from precipitation to soil saturation, runoff and last river discharge. All four locations show a rapid increase of 2-3 orders of magnitude in river flow at 09-27 12Z coinciding with the runoff peak but with a discernible lag of several hours that reflects the travel time of water through the river routing network. Jefferson/Ashe exhibits the highest peak river flow, consistent with its position draining a larger area towards bigger river routes, while Busick/Yancey shows the lowest peak, likely reflecting a smaller contributing drainage area. Importantly, unlike the runoff signal which decays to near-zero within hours, river flow remains substantially elevated through 09-30, decaying slowly over a multi-day recession characteristic of drainage following extreme flood events. In particular, Asheville/Buncombe and Jefferson/Ashe sustain the highest flow rates during this recession period, consistent with their geographic positions as the primary outlets through which accumulated water exits the flooded mountain region: Asheville draining southward into the

https://doi.org/10.5194/egusphere-2026-2014
Preprint. Discussion started: 19 May 2026

Broad River corridor and Jefferson routing flow northeastward into larger downstream networks. This is nicely captured in the snapshots at day 43 and 56. This multi-day persistence and the spatial differentiation between locations demonstrate that the river routing component is correctly integrating the upstream runoff signal and redistributing it through the drainage network on physically realistic timescales, capturing both the rapid flood onset and the slower drainage that characterized the observed Helene flooding in western North Carolina.

Taken together, these diagnostics describe a physically coherent and complete hydrological response chain: extreme precipitation from Hurricane Helene drives rapid soil saturation at both the regional and local scale, triggering saturation-excess runoff generation concentrated in a specific area, which is subsequently routed through the river network producing a multi-day flood. The timing, magnitude, and spatial distribution of each component are consistent with the physical processes expected during a catastrophic landfalling hurricane event, and with the documented impacts of Helene in western North Carolina, providing strong evidence that the land model and its coupling to the atmospheric component are functioning correctly.

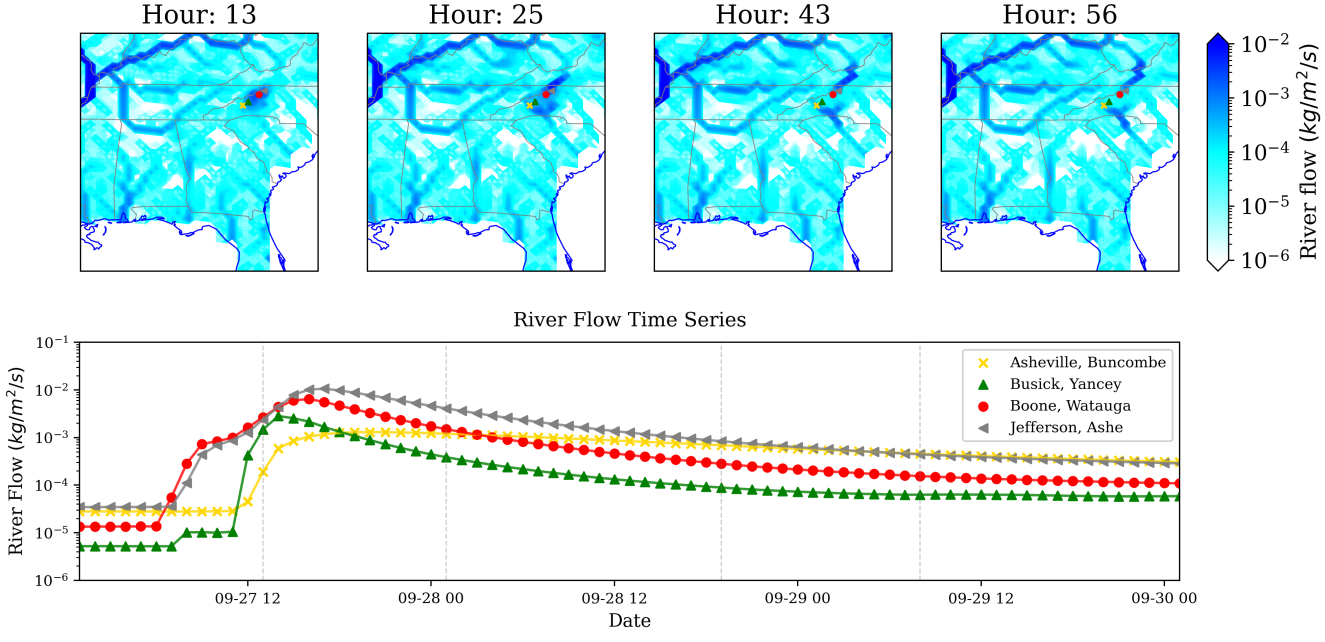

Figure 12. As for figure 9 but for river flow for hours 13, 25, 43 and 56.

5 Conclusion

We have successfully integrated GFDL's land model LM4 into SHiELD. Using the FMS coupler infrastructure, the atmospheric code and drivers were refactored to enable implicit land model coupling while maintaining modularity and flexibility. This implementation transforms SHiELD into a fully coupled Earth system model, employing MOM6/SIS2 for the ocean–sea ice system and LM4 for land and hydrological processes. Importantly, the component integration preserves the ability to run the

https://doi.org/10.5194/egusphere-2026-2014
Preprint. Discussion started: 19 May 2026

original ocean and land physics suites within the same runtime environment, using one source code and executable, ensuring backward compatibility and facilitating controlled experimentation.

The inclusion of LM4 significantly enhances the representation of land–atmosphere interactions, enabling physically consistent treatment of hydrological processes, cryospheric dynamics, soil moisture evolution, river routing, vegetation processes, and disturbance-driven aerosol emissions such as those arising from wildfires. These capabilities are essential for realistically simulating extreme hydroclimate events and compound hazards across weather to climate timescales.

We demonstrated the new configuration using the landfall of Hurricane Helene of 2024 as a case study, highlighting the land response to extreme precipitation and strong surface forcing. The evolution of soil moisture, runoff, and river discharge exhibited physically consistent behavior and qualitatively validated the the technical coupling strategy. The land surface responded dynamically to storm-driven forcing, providing confidence in the integrity of the flux exchanges and state updates across model components.

Ongoing work focuses on systematic evaluation of the fully coupled SHiELD forecast skill across multiple timescales, from short-range weather prediction to subseasonal-to-seasonal (S2S) applications. Assessments include precipitation, surface fluxes, soil moisture memory, land–atmosphere feedback strength, as well as sensitivity to land initialization, coupling frequency, and resolution, as well as the role of interactive land processes in improving forecasts at high resolution. Stability for longer lead times has also been assessed; a simulation with a lower-atmosphere resolution has integrated stably for over a year and maintained a stable climate with minimal drift, demonstrating the utility for subseasonal and longer coupled earth-system integrations.

The fully coupled SHiELD model represents a major step toward a seamless, high-resolution Earth system modeling framework. By unifying atmosphere, ocean, sea ice, and land components within a consistent infrastructure, this development lays the foundation for improved prediction of extreme events, enhanced understanding of cross-component feedbacks, and a more integrated approach to weather–climate research.

Code availability. The fully coupled SHiELD model is under active development and can be built and run from the latest official releases from the NOAA-GFDL GitHub repository. The source files used in this study are available at https://doi.org/10.5281/zenodo.19476778 Mouallem (2026)

Competing interests. The authors declare that they have no conflict of interest.

Disclaimer. The statements, findings, conclusions, and recommendations are those of the author(s) and do not necessarily reflect the views of the National Oceanic and Atmospheric Administration, or the US Department of Commerce.

https://doi.org/10.5194/egusphere-2026-2014
Preprint. Discussion started: 19 May 2026

Acknowledgements. We thank Laura Torres Rojas and Youngji Joh for their review, discussion and useful comments that improved the quality of the manuscript. Joseph Mouallem, Kun Gao and Zhihong Tan are supported under awards NA18OAR4320123, NA23OAR4320198, NA23OAR4050432I from the National Oceanic and Atmospheric Administration, U.S. Department of Commerce. This work is also supported by the NOAA research Global-Nest Initiative and the Bipartisan Infrastructure Law (BIL).

https://doi.org/10.5194/egusphere-2026-2014
Preprint. Discussion started: 19 May 2026

References

Adcroft, A., Anderson, W., Balaji, V., Blanton, C., Bushuk, M., Dufour, C. O., Dunne, J. P., Griffies, S. M., Hallberg, R., Harrison, M. J., Held, I. M., Jansen, M. F., John, J. G., Krasting, J. P., Langenhorst, A. R., Legg, S., Liang, Z., McHugh, C., Radhakrishnan, A., Reichl, B. G., Rosati, T., Samuels, B. L., Shao, A., Stouffer, R., Winton, M., Wittenberg, A. T., Xiang, B., Zadeh, N., and Zhang, R.: The GFDL Global Ocean and Sea Ice Model OM4.0: Model Description and Simulation Features, Journal of Advances in Modeling Earth Systems, 11, 3167–3211, https://doi.org/10.1029/2019MS001726, 2019.

Balaji, V.: The Flexible Modeling System, pp. 33–41, Springer Berlin Heidelberg, Berlin, Heidelberg, https://doi.org/10.1007/978-3-642-23360-9_5, 2012.

Balaji, V. and Langenhorst, A.: ESM Workflow, pp. 5–13, Springer Berlin Heidelberg, Berlin, Heidelberg, https://doi.org/10.1007/978-3-642-23932-8_2, 2012.

Balaji, V., Anderson, J., Held, I., Winton, M., Durachta, J., Malyshev, S., and Stouffer, R. J.: The Exchange Grid: A mechanism for data exchange between Earth System components on independent grids, in: Parallel Computational Fluid Dynamics 2005, edited by Deane, A., Ecer, A., McDonough, J., Satofuka, N., Brenner, G., Emerson, D. R., Periaux, J., and Tromeur-Dervout, D., pp. 179–186, Elsevier, Amsterdam, https://doi.org/0.1016/B978-044452206-1/50021-5, 2006.

Chen, X., Andronova, N., Leer, B. V., Penner, J. E., Boyd, J. P., Jablonowski, C., and Lin, S. J.: A control-volume model of the compressible Euler equations with a vertical Lagrangian coordinate, Monthly Weather Review, 141, 2526–2544, https://doi.org/10.1175/MWR-D-12-00129.1, 2013.

Delworth, T. L., Cooke, W. F., Adcroft, A., Bushuk, M., Chen, J.-H., Dunne, K. A., Ginoux, P., Gudgel, R., Hallberg, R. W., Harris, L., Harrison, M. J., Johnson, N., Kapnick, S. B., Lin, S.-J., Lu, F., Malyshev, S., Milly, P. C., Murakami, H., Naik, V., Pascale, S., Paynter, D., Rosati, A., Schwarzkopf, M., Shevliakova, E., Underwood, S., Wittenberg, A. T., Xiang, B., Yang, X., Zeng, F., Zhang, H., Zhang, L., and Zhao, M.: SPEAR: The Next Generation GFDL Modeling System for Seasonal to Multidecadal Prediction and Projection, Journal of Advances in Modeling Earth Systems, 12, e2019MS001 895, https://doi.org/https://doi.org/10.1029/2019MS001895, e2019MS001895 2019MS001895, 2020.

Ek, M. B., Mitchell, K. E., Lin, Y., Rogers, E., Grunmann, P., Koren, V., Gayno, G., and Tarpley, J. D.: Implementation of Noah land surface model advances in the National Centers for Environmental Prediction operational mesoscale Eta model, Journal of Geophysical Research: Atmospheres, 108, https://doi.org/10.1029/2002JD003296, 2003.

F. Santos, L., Mouallem, J., and S. Peixoto, P.: Analysis of finite-volume transport schemes on cubed-sphere grids and an accurate scheme for divergent winds, Journal of Computational Physics, 522, 113 618, https://doi.org/https://doi.org/10.1016/j.jcp.2024.113618, 2025.

Han, J. and Bretherton, C. S.: TKE-Based Moist Eddy-Diffusivity Mass-Flux (EDMF) Parameterization for Vertical Turbulent Mixing, Weather and Forecasting, 34, 869 – 886, https://doi.org/10.1175/WAF-D-18-0146.1, 2019.

Han, J., Wang, W., Kwon, Y. C., Hong, S.-Y., Tallapragada, V., and Yang, F.: Updates in the NCEP GFS Cumulus Convection Schemes with Scale and Aerosol Awareness, Weather and Forecasting, 32, 2005 – 2017, https://doi.org/10.1175/WAF-D-17-0046.1, 2017.

Harris, L., Zhou, L., Lin, S. J., Chen, J. H., Chen, X., Gao, K., Morin, M., Rees, S., Sun, Y., Tong, M., Xiang, B., Bender, M., Benson, R., Cheng, K. Y., Clark, S., Elbert, O. D., Hazelton, A., Huff, J. J., Kaltenbaugh, A., Liang, Z., Marchok, T., Shin, H. H., and Stern, W.: GFDL SHiELD: A Unified System for Weather-to-Seasonal Prediction, Journal of Advances in Modeling Earth Systems, 12, 1–25, https://doi.org/10.1029/2020MS002223, 2020.

https://doi.org/10.5194/egusphere-2026-2014
Preprint. Discussion started: 19 May 2026

Harris, L. M. and Lin, S. J.: A two-way nested global-regional dynamical core on the cubed-sphere grid, Monthly Weather Review, 141, 283–306, https://doi.org/10.1175/MWR-D-11-00201.1, 2013.

Harris, L. M., Lin, S.-J., and Tu, C.: High-Resolution Climate Simulations Using GFDL HiRAM with a Stretched Global Grid, https://doi.org/10.1175/JCLI-D-15-0389.s1, 2016.

Held, I. M., Guo, H., Adcroft, A., Dunne, J. P., Horowitz, L. W., Krasting, J., Shevliakova, E., Winton, M., Zhao, M., Bushuk, M., Wittenberg, A. T., Wyman, B., Xiang, B., Zhang, R., Anderson, W., Balaji, V., Donner, L., Dunne, K., Durachta, J., Gauthier, P. P. G., Ginoux, P., Golaz, J.-C., Griffies, S. M., Hallberg, R., Harris, L., Harrison, M., Hurlin, W., John, J., Lin, P., Lin, S.-J., Malyshev, S., Menzel, R., Milly, P. C. D., Ming, Y., Naik, V., Paynter, D., Paulot, F., Ramaswamy, V., Reichl, B., Robinson, T., Rosati, A., Seman, C., Silvers, L. G., Underwood, S., and Zadeh, N.: Structure and Performance of GFDL's CM4.0 Climate Model, Journal of Advances in Modeling Earth Systems, 11, 3691–3727, https://doi.org/10.1029/2019MS001829, 2019.

Lin, S. J.: A "vertically Lagrangian" finite-volume dynamical core for global models, Monthly Weather Review, 132, 2293–2307, https://doi.org/10.1175/1520-0493(2004)132<2293:AVLFDC>2.0.CO;2, 2004.

Lin, S.-J. and Rood, R. B.: Multidimensional Flux-Form Semi-Lagrangian Transport Schemes, Monthly Weather Review, 124, 2046 – 2070, https://doi.org/10.1175/1520-0493(1996)124<2046:MFFSLT>2.0.CO;2, 1996.

Lin, S.-J. and Rood, R. B.: An explicit flux-form semi-Lagrangian shallow-water model on the sphere, Quarterly Journal of the Royal Meteorological Society, 123, 2477–2498, https://doi.org/https://doi.org/10.1002/qj.49712354416, 1997.

Mouallem, J.: Development of a high-resolution coupled SHiELD- MOM6-LM4 model – Part 2: Model overview, coupling technique, and evaluation of hydrological extremes during Hurricane Helene, https://doi.org/10.5281/zenodo.19476778, 2026.

Mouallem, J., Harris, L., and Benson, R.: Multiple same-level and telescoping nesting in GFDL's dynamical core, Geoscientific Model Development, 15, 4355–4371, https://doi.org/10.5194/gmd-15-4355-2022, 2022.

Mouallem, J., Harris, L., and Chen, X.: Implementation of the Novel Duo-Grid in GFDL's FV3 Dynamical Core, Journal of Advances in Modeling Earth Systems, 15, e2023MS003 712, https://doi.org/https://doi.org/10.1029/2023MS003712, e2023MS003712 2023MS003712, 2023.

Mouallem, J., Gao, K., Reichl, B. G., Chilutti, L., Harris, L., Benson, R., Zadeh, N., Chen, J., Chen, J.-H., and Zhang, C.: Development of a High-Resolution Coupled SHiELD- MOM6 Model. Part I – Model Overview, Coupling Technique, and Validation in a Regional Setup, Geoscientific Model Development, 18, 6461–6478, https://doi.org/10.5194/gmd-18-6461-2025, 2025.

Niu, G.-Y., Yang, Z.-L., Mitchell, K. E., Chen, F., Ek, M. B., Barlage, M., Kumar, A., Manning, K., Niyogi, D., Rosero, E., Tewari, M., and Xia, Y.: The community Noah land surface model with multiparameterization options (Noah-MP): 1. Model description and evaluation with local-scale measurements, Journal of Geophysical Research: Atmospheres, 116, https://doi.org/10.1029/2010JD015139, 2011.

O'Neill, B. C., Tebaldi, C., van Vuuren, D. P., Eyring, V., Friedlingstein, P., Hurtt, G., Knutti, R., Kriegler, E., Lamarque, J.-F., Lowe, J., Meehl, G. A., Moss, R., Riahi, K., and Sanderson, B. M.: The Scenario Model Intercomparison Project (ScenarioMIP) for CMIP6, Geosci. Model Dev., 9, 3461–3482, https://doi.org/https://doi.org/10.5194/gmd-9-3461-2016, 2016.

Pollard, R. T., Rhines, P. B., and Thompson, R. O. R. Y.: The deepening of the wind-Mixed layer, Geophysical Fluid Dynamics, 4, 381–404, https://doi.org/10.1080/03091927208236105, 1973.

Putman, W. M. and Lin, S. J.: Finite-volume transport on various cubed-sphere grids, Journal of Computational Physics, 227, 55–78, https://doi.org/10.1016/j.jcp.2007.07.022, 2007.

https://doi.org/10.5194/egusphere-2026-2014
Preprint. Discussion started: 19 May 2026

van Vuuren, D., Kriegler, E., O'Neill, B., K.L., E., K., R., R., C. T., J., E., S., H., T., K., R., M., and H., W.: A new scenario framework for Climate Change Research: scenario matrix architecture., Climatic Change, 122, 373–386, https://doi.org/https://doi.org/10.1007/s10584-013-0906-1, 2014.

Zhao, M., Golaz, J.-C., Held, I. M., Guo, H., Balaji, V., Benson, R., Chen, J.-H., Chen, X., Donner, L. J., Dunne, J. P., Durachta, J. W., Fan, S.-M., Friedenreich, S. M., Garner, S. T., Ginoux, P., Harris, L. M., Horowitz, L. W., Krasting, J. P., Langenhost, A. R., Liang, Z., Lin, P., Lin, S.-J., Malyshev, S., Mason, E., Milly, P. C. D., Ming, Y., Naik, V., Paulot, F., Paynter, D., Phillips, P. J., Radkhakrishnan, A., Ramaswamy, V., Robinson, T., Schwarzcopf, M. D., Seman, C. J., Shevliakova, E., Shen, Z., Shin, H., Silvers, L. G., Wilson, J. R., Winton, M., Wittenberg, A. T., Wyman, B. L., and Xiang, B.: The GFDL Global Atmosphere and Land Model AM4.0/LM4.0: 2. Model Description, Sensitivity Studies, and Tuning Strategies, Journal of Advances in Modeling Earth Systems, 10, 735–769, https://doi.org/10.1002/2017ms001209, 2018.

Zhou, L., Harris, L., and Chen, J.-H.: The GFDL Cloud Microphysics Parameterization, NOAA technical memorandum OAR GFDL ; 2022-002, https://doi.org/10.25923/pz3c-8b96, 2022a.

Zhou, L., Harris, L., Chen, J.-H., Gao, K., Guo, H., Xiang, B., Tong, M., Huff, J. J., and Morin, M.: Improving Global Weather Prediction in GFDL SHiELD Through an Upgraded GFDL Cloud Microphysics Scheme, Journal of Advances in Modeling Earth Systems, 14, https://doi.org/10.1029/2021MS002971, 2022b.